

METEOROLOGICAL SATELLITE CENTER
TECHNICAL NOTE

No.66 (2022)

METEOROLOGICAL SATELLITE CENTER
235, Nakakiyoto 3 Chome, Kiyose-shi
Tokyo 204-0012, JAPAN
OCTOBER 2022

Himawari-8 Fog Detection Product Development

MARUYAMA Takumi*¹, ISHIDA Haruma*², CHUBACHI Koetsu*³

Abstract

Fog monitoring is critical for safety in the areas of aviation, maritime navigation and road travel. Satellite observation provides wide coverage in monitoring of fog distribution over land and sea surfaces, but this technique alone does not allow effective discrimination between fog and low cloud (i.e., whether the cloud bottom touches the ground) because of its aerial nature. To address this issue, JMA's Himawari-8 Fog product incorporates numerical weather prediction data for altitudes around the ground surface in addition to Himawari-8 observation results, thereby creating two-dimensional information for determining the presence of fog. This report describes the product's algorithm, accuracy and considerations to be noted in usage.

1. Introduction

Information on fog areas is important for safety in aviation, marine navigation and road travel. In this regard, ground-based monitoring (e.g., visual observation and automated observation using visibility meters and live cameras) is useful. However, the information it produces relates only to areas near observation sites because fog distribution is characterized by high locality. Forecasting and air traffic control involving overall fog areas and related flow over land and sea requires information covering wider regions. Satellite observation provides global surface information covering both sea and land surfaces, and areas of low cloud (which may include fog) can be displayed with 2D distribution in RGB composite imagery using the data produced (e.g., Shimizu 2020). However, this technique is not ideal for distinguishing between fog and low clouds (i.e., whether the cloud bottom touches the ground) because it involves observation from

altitude. Against such a background, JMA's Himawari-8 fog detection product (referred to here simply as the "Fog product") combines numerical weather prediction (NWP) data for areas around ground-surface altitude with Himawari-8 observation data (Bessho et al. 2016), creating information on fog over the whole of the earth's surface. Fog product development is based on related research using satellite observation data and NWP data as per Ishida et al. (2014).

This report outlines the Fog product (Chapter 2), the algorithm used (Chapter 3) and related accuracy (Chapter 4). Further descriptions are provided on usage (Chapter 5) and future development (Chapter 6) before the conclusion (Chapter 7).

2. Fog product outline

Fog product examples are shown in Figures 1 (a), (b) and (c). Fog areas are shown in orange against the infrared

*¹ Office of Meteorological Analysis and Application Development, Administration Division, Atmosphere and Ocean Department, Japan Meteorological Agency

*² Department of Observation and Data Assimilation Research, Meteorological Research Institute

*³ HALEX CORPORATION

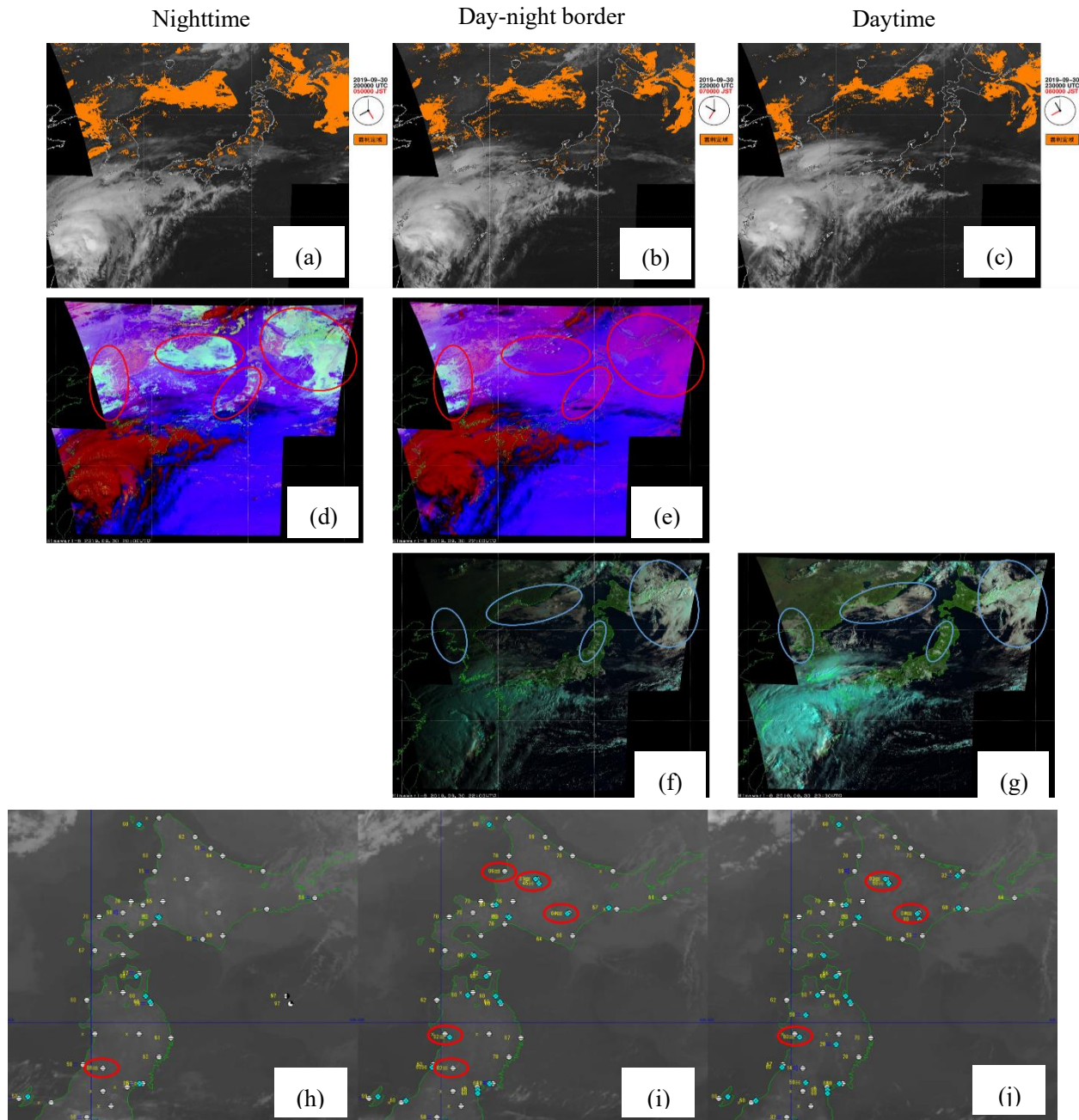


Figure 1: Fog product display

(a), (b), (c): Fog product imagery; (d), (e): Night Microphysics RGB composite imagery; (f), (g): Natural Color RGB composite imagery; (h), (i), (j): Weather and visibility for ground observation points (red circles: fog observation points). (a), (d): 20 UTC on 30th September (nighttime); (b), (e), (f): 22 UTC, 30th September (day-night border); (c), (g): 23 UTC on 30th September (daytime) 2019.

imagery background (B13). The product provides information on Japan and the surrounding area for aviation usage, with a spatial resolution of 0.02° and a temporal resolution of 5 min. The NWP employed is the Meso-Scale

Model (MSM) (JMA, 2022), the forecast time is three hours or longer with temporal interpolation, and the initial time is switched to the latest forecast every three hours (00, 03, 06, 09, 12, 15, 18, 21 UTC). Fog is observed at multiple

Table 1: Satellite observation data utilized in the Fog product

Satellite observation data (Himawawri-8/9)			Fog product usage		
Band	Central Wavelength [μm]	Spatial Resolution [km]	Day	Night	
B01	0.47	1			
B02	0.51				
B03	0.64	0.5	○		
B04	0.86	1	○		
B05	1.6	2	○		
B06	2.3				
B07	3.9				
B08	6.2			○	
B09	6.9				
B10	7.3				
B11	8.6				
B12	9.6				
B13	10.4			○	○
B14	11.2				
B15	12.4				
B16	13.3				

Table 2: Fog product NWP data

NWP data (MSM : Meso-Scale Model)
Temperature (Ground, 700 hPa)
Relative humidity (Ground, 925 hPa, 850 hPa, 700 hPa)

ground sites in Hokkaido (Japan’s northernmost major island) and the Tohoku region (northern mainland Japan) shown with red circles in Figures 1 (h), (i) and (j).

For comparison, Night Microphysics RGB composite imagery (useful for nighttime cloud/fog identification) is shown in Figures 1 (d) and (e), and Natural Color RGB composite imagery (useful for daytime identification) is shown in Figures 1 (f) and (g) (See Shimizu 2020 for details of color interpretation). Night Microphysics RGB composite imagery clearly shows low clouds/fog in light blue for nighttime (red circles in Figure 1 (d)), but this is unclear at times on the day-night border (Figure 1 (e)). Natural Color RGB composite imagery clearly shows low clouds/fog in light grey for daytime (blue circles in Figure 1 (g)), but this is also unclear at times on the day-night

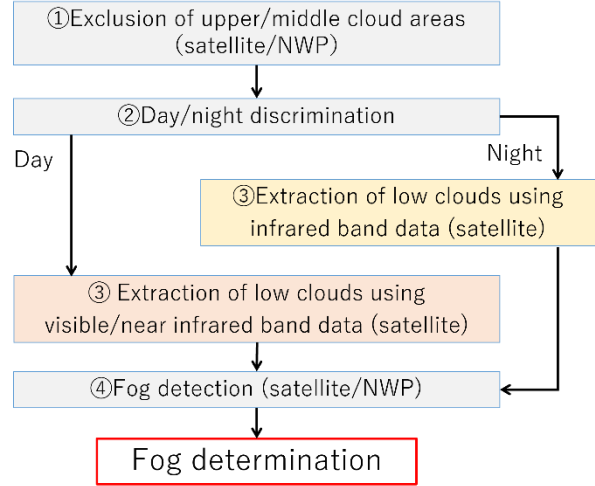


Figure 2: Fog determination flow chart

Table 3: Fog product threshold settings

① Exclusion of upper/middle clouds	$T_{B13} > {}_{nwp}T_{700hPa}$
	${}_{nwp}RH_{700hPa} < 90$ [%]
② Day/night discrimination	Day : $SZA < 87$ [deg]
	Night : $SZA \geq 87$ [deg]
③ Extraction of low clouds	Day : $R_{B03}/\cos(SZA) \geq 0.3$
	Night : $R_{B05}/R_{B04} \geq 0.5$
④ Fog determination	$T_{B07} - T_{B13} \leq -1.5$
	${}_{nwp}T_{surf} - T_{B13} \leq 10$
	$T_{B13} \geq -10$ [°C]
	${}_{nwp}RH_{surf} \geq 85$ [%]
	${}_{nwp}RH_{surf} \geq {}_{nwp}RH_{max}(700/850/925hPa)$

border (Figure 1 (f)). The Fog product mostly corresponds to the light-blue areas in Night Microphysics RGB composite imagery for the nighttime, and light-grey areas in Natural Color RGB composite imagery for the daytime. The Fog product also shows fog areas well for times on the day-night border.

Color tones in fog monitoring using RGB composite imagery are affected by sunlight on the day-night border (i.e., at sunrise and sunset), which necessitates checking of multiple images in parallel. The Fog product eliminates this need for differences between day and night.

3. Fog product algorithms

This chapter details the Fog product algorithms. Tables 1

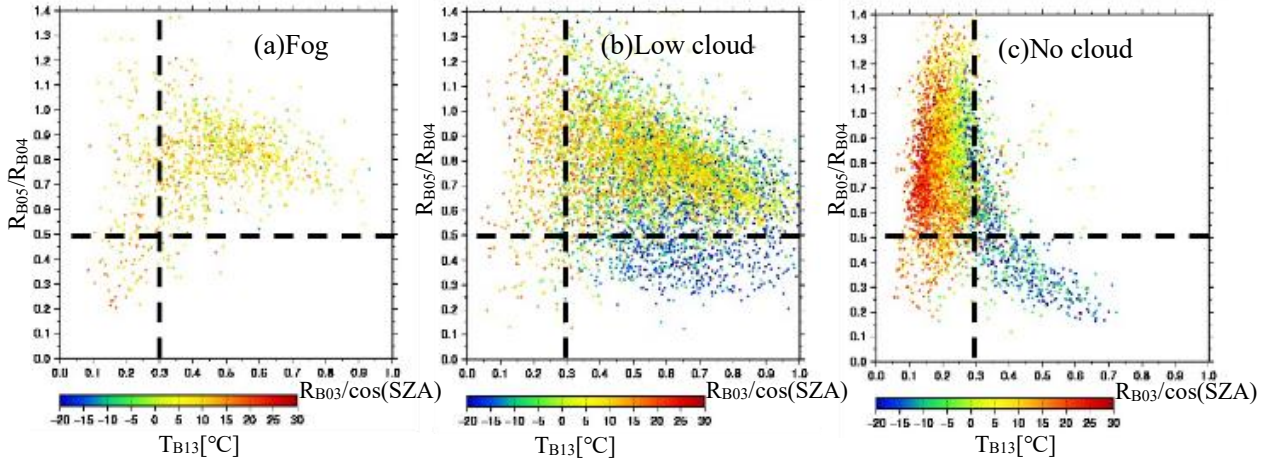


Figure 3: Scatter plots of $R_{B03}/\cos(\text{SZA})$ and R_{B05}/R_{B04} in the nearest grid to the SYNOP observation site in the daytime ($\text{SZA} < 87$ [deg]) between August 2015 and July 2016

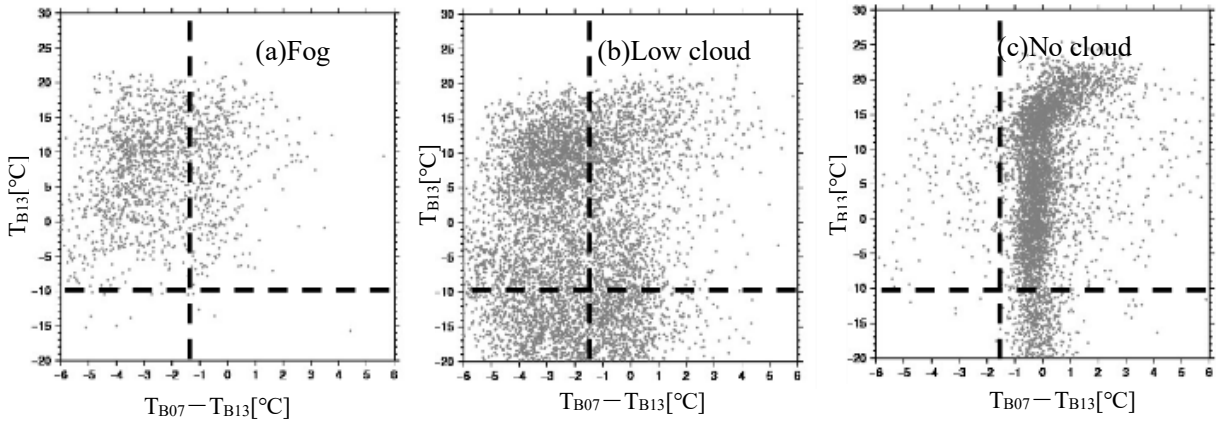


Figure 4: Scatter plots of $T_{B07} - T_{B13}$ and T_{B13} in the nearest grid to the SYNOP observation site at nighttime ($\text{SZA} \geq 87$ [deg]) between August 2015 and July 2016

and 2 list the observation bands of Himawari-8 and the NWP (MSM) data used. The product determines fog with set thresholds on values derived from satellite observation and NWP. For threshold setting, data from August 2015 to July 2016 were used. For product accuracy monitoring as described in Section 4, data from August 2016 to July 2017 were used.

3.1. Threshold setting

Setting was based on observed incidences of fog, low cloud (stratocumulus, stratus, cumulus, cumulonimbus)/cloudy, and no cloud (cloud amount 0) as extracted from SYNOP and SHIP visual observation

records, which are numerical codes used for reporting of surface observations. At the nearest grid to the visual observation site, data from satellite observation and NWP were characterized for each incidence. The distance between the visual observation site and the nearest neighbor grid is 0.01° or less in each of the latitude and longitude directions. As the product specifically targets fog, thresholds were also set to discriminate fog from low cloud/cloudy.

3.2. Fog determination

Figure 2 highlights the product formulation procedures, and Table 3 summarizes the discrimination thresholds (see

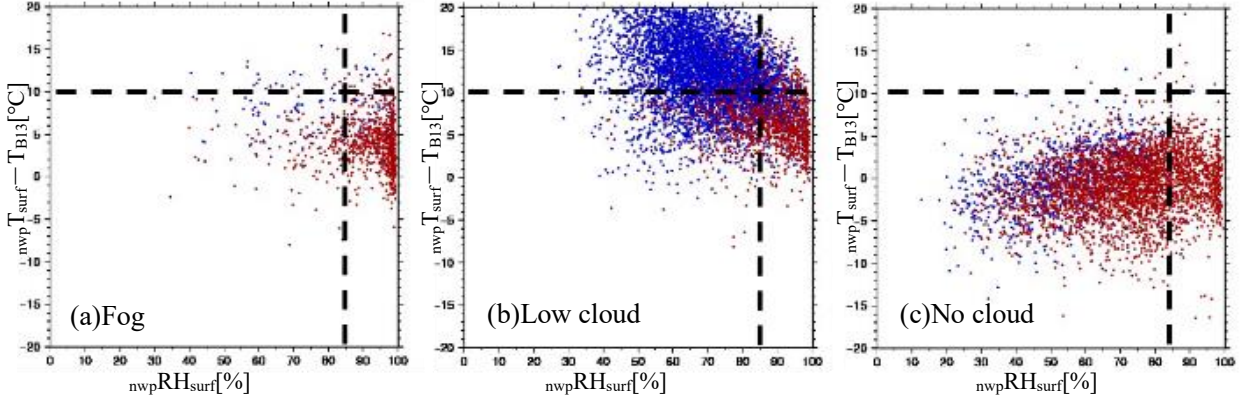


Figure 5: Scatter plots of $nwpRH_{surf}$ and $nwpT_{surf} - T_{B13}$ in the nearest grid to the SYNOP observation site in the daytime ($SZA < 87 [deg]$) between August 2015 and July 2016 ($nwpRH_{surf} \geq nwpRH_{max}(700/850/925hPa)$ in red, $nwpRH_{surf} < nwpRH_{max}(700/850/925hPa)$ in blue)

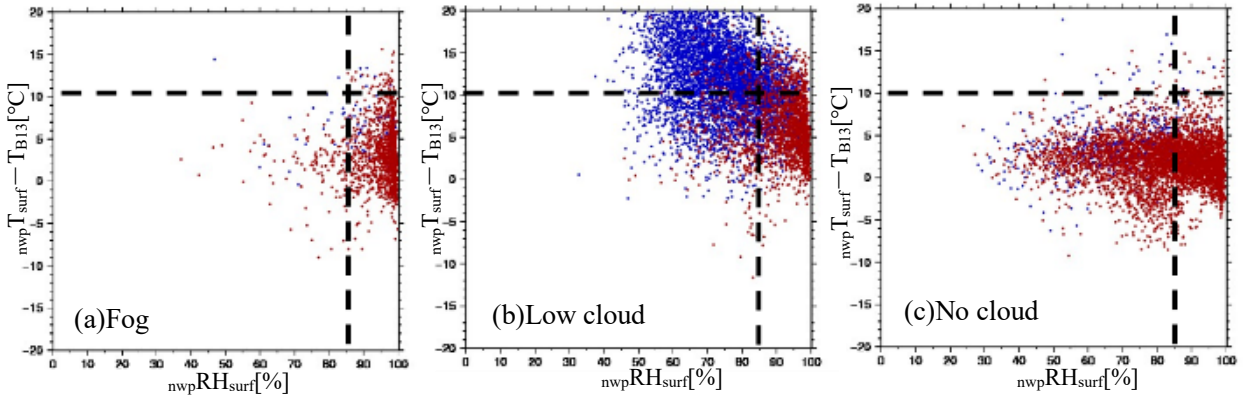


Figure 6: As per Figure 5, but for nighttime ($SZA \geq 87 [deg]$)

appendix for legend).

As a prerequisite for fog detection, the absence of upper and mid-level clouds is determined using T_{B13} , $nwpT_{700hPa}$ and $nwpRH_{700hPa}$, and day-night discrimination is then performed with reference to SZA to decide appropriate satellite observation bands for use in low-cloud identification. For daytime hours, B03, B04 and B05 (used for Natural Color RGB composite imagery), should be selected; for nighttime hours, B07 and B13 (used for Night Microphysics RGB composite imagery) should be used.

Figure 3 shows $R_{B03}/\cos(SZA)$ and R_{B05}/R_{B04} values for the nearest SYNOP observation point in the daytime ($SZA < 87 [deg]$) between August 2015 and July 2016. The target area was $22.4 - 47.6^\circ N$ and $120.0 - 150.0^\circ E$, and plots were made separately for fog, low cloud/cloudy and no

cloud. Based on the results, daytime thresholds were determined for identification of low cloud/fog areas. The dashed line in the figure indicates the product thresholds. As visible reflectance is generally higher in cloudy areas than in clear areas (e.g., Shimizu et al. 2017), $R_{B03}/\cos(SZA) \geq 0.3$ was set as one condition. Since visible reflectance is high both in cloud areas and in those with snow and ice (e.g., Shimizu et al. 2017), erroneous detection may occur with the condition of $R_{B03}/\cos(SZA)$ only. As per $R_{B03}/\cos(SZA) \geq 0.3$ region in Figure 3 (c), the color of T_{B13} tends to be observed with sub-zero temperatures, indicating a potential snow ice area. In the wavelength region of near-infrared corresponding to B05, the reflectance of ice cloud/snow ice areas is lower than that of water cloud (e.g., Shimizu et al. 2017). Accordingly,

Table 4: Evaluation of Fog product with SYNOP and SHIP (Aug 2016 – Jul 2017)

Threat score = $FO/(FO+FX+XO)$ Hit rate = $(FO+XX)/N$ False alarm rate = $FX/(FO+FX)$ Miss rate = XO/M					
		Fog product (with MSM)			
		Day		Night	
		SYNOP (land)	SHIP (sea)	SYNOP (land)	SHIP (sea)
Incidences		11707	1047	12676	913
Fog observation		887	33	1245	37
Threat score		0.306	0.237	0.324	0.375
Hit rate		0.913	0.945	0.880	0.962
False alarm rate		0.562	0.705	0.580	0.475
Miss rate		0.496	0.455	0.413	0.432
		SYNOP/SHIP fog observation		Total	
		Fog	No fog		
Fog product-based determination	Detected	Hit (FO)	False alarm (FX)	FO+FX	
	Not detected	Miss (XO)	Hit (XX)	XO+XX	
Total		M	X	N	

Table 5: Fog product result evaluation with SYNOP comparison by season (Autumn: Sep. – Nov. 2016; winter: Dec. 2016 – Feb. 2017; spring: Mar. – May 2017; summer: Jun. – Aug. 2017)

		Fog product (with MSM)							
		Day				Night			
Season		Autumn	Winter	Spring	Summer	Autumn	Winter	Spring	Summer
Incidences		2351	4378	2857	2192	3181	4807	2795	1737
Fog observation		133	118	200	370	347	178	292	376
Threat score		0.210	0.204	0.344	0.329	0.336	0.278	0.308	0.330
Hit rate		0.931	0.962	0.924	0.796	0.876	0.945	0.864	0.732
False alarm rate		0.626	0.684	0.535	0.575	0.554	0.649	0.602	0.582
Miss rate		0.677	0.636	0.430	0.405	0.424	0.427	0.421	0.388

the condition of $R_{B05}/R_{B04} \geq 0.5$ was added to avoid erroneous detection due to snow ice. However, as this condition does not support detection of both ice fog and snow ice areas, the current fog product targets water-droplet fog only. Figure 4 illustrates $T_{B07} - T_{B13}$ and T_{B13} for nighttime hours ($SZA \geq 87[\text{deg}]$), and thresholds for low cloud detection were based on these results. As T_{B07} is lower than T_{B13} in low cloud areas consisting of water droplets (e.g., Ellrod 1995), $T_{B07} - T_{B13} \leq -1.5$ was set as the threshold. In Figure 4 (a), T_{B13} exceeds -10°C in most fog cases. Accordingly, the threshold of $T_{B13} \geq -10^\circ\text{C}$ was added to reduce the number of detections without fog.

After satellite data-based identification of low cloud areas that may include fog, final identification is performed using NWP data. Figures 5 and 6 show ${}_{\text{nwp}}RH_{\text{surf}}$ and ${}_{\text{nwp}}T_{\text{surf}} - T_{B13}$ for day and night, respectively. The thresholds used to identify fog areas were based on these results. Notably for ${}_{\text{nwp}}RH_{\text{surf}}$, values are over 85% for most

fog incidences. Accordingly, ${}_{\text{nwp}}RH_{\text{surf}} \geq 85\%$ was set as the threshold for fog indication. For ${}_{\text{nwp}}T_{\text{surf}} - T_{B13}$, the difference was smaller for fog than for low clouds (i.e., ${}_{\text{nwp}}T_{\text{surf}}$ and T_{B13} were closer). Accordingly, ${}_{\text{nwp}}T_{\text{surf}} - T_{B13} \leq 10^\circ\text{C}$ was set as another threshold for fog. In comparison made for humidity as derived from NWP in the 700/850/925 hPa and ground layers, the highest humidity was seen at the ground surface in fog incidences. Accordingly, the condition of ${}_{\text{nwp}}RH_{\text{surf}} \geq {}_{\text{nwp}}RH_{\text{max}(700/850/925\text{hPa})}$ was added.

With the threshold settings shown in Table 3, the ratios of fog observations in SYNOP to fog detections with the Fog product were 47% for daytime and 47% for nighttime during the threshold survey period (August 2015 to July 2016). The ratio of low cloud observations in SYNOP to fog detections with the Fog product was 47% for daytime and 45% for nighttime.

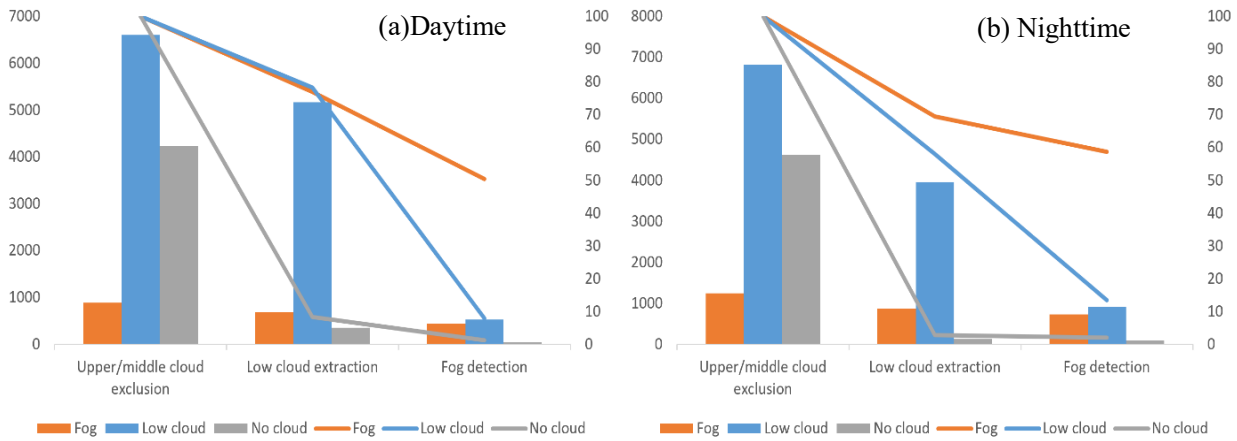


Figure 7: Extraction cases (bars: left axis) and extraction ratios (%) (polygonal lines: right axis) for fog, low cloud and no cloud in each process of the fog determination shown in Figure 2

(a) Nearest grid to the SYNOP observation site for daytime ($SZA < 87$ [deg]) between August 2016 and July 2017

(b) As per Figure 7 (a), but for nighttime ($SZA \geq 87$ [deg])

4. Fog product accuracy

This chapter outlines Fog product evaluation and the results obtained.

4.1. Accuracy evaluation

The Fog product was evaluated by comparing results against SYNOP and SHIP data. The product grid evaluated was that nearest the visual ground observation site, with exclusion of upper and middle cloud identified in the first step of fog determination. The evaluation area was $22.4 - 47.6^\circ\text{N}$ and $120.0 - 150.0^\circ\text{E}$.

4.2. Evaluation results by day/night and by sea/land

Table 4 summarizes the evaluation results by day/night and by sea/land for the period between August 2016 and July 2017. Comparisons with SYNOP and SHIP data were regarded as evaluations for land and sea, respectively. Overall, 59% (daytime) and 52% (nighttime) of fog incidences were not detected due to the presence of upper and middle clouds in fog determination as compared to all cases in SYNOP fog observation. Hit rates were all above 80% for day/night and sea/land, indicating a high hit rate

for no fog. In evaluating hit rates for fog, focus was placed on threat scores. Although sea surface daytime scores were worse, values were around 0.3 for day/night and sea/land, indicating roughly even accuracy regardless of time zones and surface conditions. The undetected miss ratio was around 40 – 50%, and the false alarm ratio was around 50 – 70%.

4.3. Evaluation results by season

Table 5 shows evaluation results by day/night and by season for land. Worse threat score results were seen in winter for both day and night. Since fewer fog incidences were observed and the false alarm ratio was higher in winter, it is considered that erroneous fog detection for low cloud not including fog tended to occur. The higher winter miss ratio may be attributable to the current algorithm's inability to detect ice fog (see Chapter 5 b).

4.4. Validation of the fog determination flow chart

Figure 7 shows numbers of extraction cases and extraction ratios for fog, low cloud/cloudy and no cloud in each process of fog determination (upper/middle cloud exclusion, low cloud extraction and fog detection). Here,

Table 6: Fog product result evaluation with SYNOP comparison for the case up to the low-cloud extraction process shown in Figure 2 (Aug 2016 – Jul 2017)

SYNOP	Fog product	
	Day	Night
Incidences	11707	12676
Fog observed	887	1245
Threat score	0.107	0.162
Hit rate	0.511	0.648
False alarm rate	0.890	0.825
Miss rate	0.231	0.306

the extraction ratio is defined as the ratio of the number of extracted cases after low cloud extraction or fog detection to the number of cases after upper/middle cloud exclusion. Focusing on the extraction ratio for fog (orange polygonal lines), low cloud extraction misidentified 23% of daytime fog cases and 31% of nighttime cases as clear weather (corresponding to the reduction of polygonal lines due to low cloud extraction). In association with subsequent fog detection processing, 27% of daytime fog cases and 10% of nighttime cases were judged as low cloud (corresponding to the reduction of polygonal lines due to fog detection), and the final extraction ratios for fog (right end of the orange polygonal lines) were 50% for daytime and 59% for nighttime. Extraction ratios for no cloud after fog detection (right end of the grey polygonal lines) were 1% for daytime and 2% for nighttime, while those for low cloud/cloudy (right end of the blue polygonal lines) were 8% for daytime and 13% for nighttime. It can therefore be considered that in false detection, low cloud extraction was successful and low clouds (not fog) were mainly misidentified as fog.

In Figure 2, the threat score evaluated with SYNOP when the detection result up to low cloud extraction (no fog) was 0.107 for daytime and 0.162 for nighttime, as shown in Table 6. Compared to the threat scores in Table 4 (0.306 for daytime and 0.324 for nighttime) a combination of satellite data and numerical weather prediction data

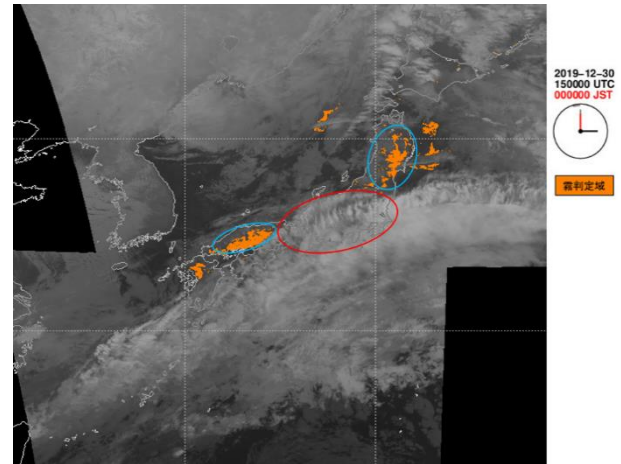


Figure 8: Fog product display with upper/middle clouds (15 UTC, 30th December 2019)

shows threat scores around 2.9 times higher for daytime and around 2.0 for nighttime.

5. Notes on product usage

The following points should be noted.

- No detection of fog under upper and middle clouds
As judgement is based on satellite observation, fog invisible to satellites cannot be detected. Figure 8 shows a Fog product display with upper and middle clouds present. Fog was observed here at multiple ground stations in mainland Japan from the Tohoku region to the Chugoku region. The product detected fog in both regions, as shown by the blue circles. In regions surrounded by red circles, such as the Kanto/Koshin region, infrared (B13) imagery shows whitish areas, and fog was not detected because of upper/middle clouds.
- No detection of ice fog
As low ice cloud (including ice fog) and snow ice areas appear nearly identical and are hard to discriminate in satellite observation, only fog exclusively consisting of water is detected.
- Dependence of detection accuracy on NWP model precision
As fog identification in the product involves the use of NWP model predictions, accuracy may be impaired if

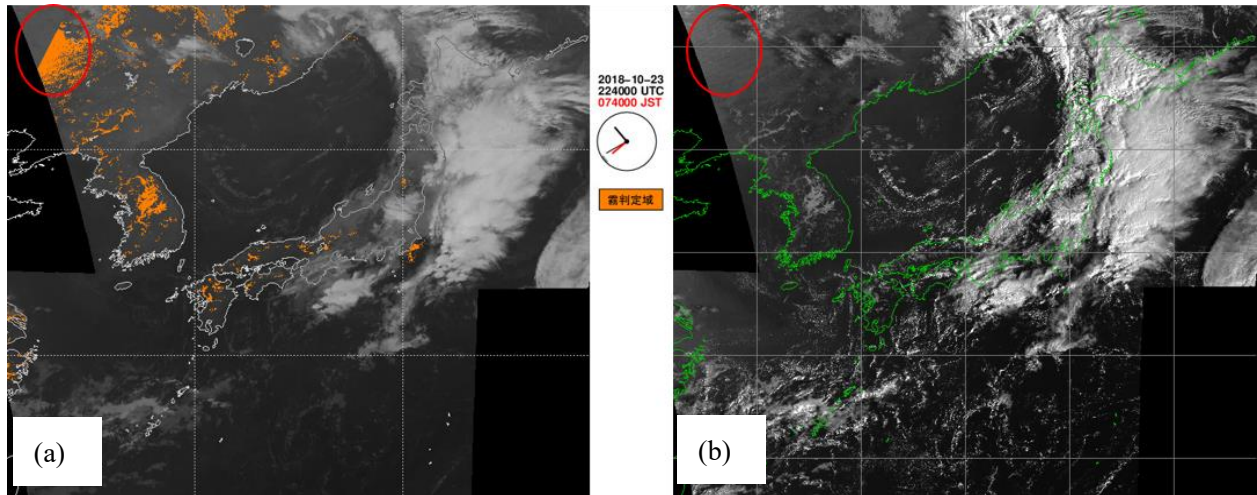


Figure 9: Erroneous fog product detection (2240 UTC, 23rd October 2018)

(a: Fog product; b : $R_{B03}/\cos(SZA)$ imagery)

these predictions differ greatly from actual values.

d) Difficulty of detecting local fog areas too small for satellite spatial resolution and very thin fog

The characteristics of fog areas smaller than the horizontal resolution of Himawari-8 (around 2 km at the sub-satellite point in infrared bands) cannot be readily captured. Extremely thin fog through which the ground is visible is also difficult to accurately characterize in satellite observation, and may remain undetected.

e) Tendency for false detection at sunrise and sunset

Figure 9 shows an example of false fog detection at sunrise. The product results in Figure 9 (a) show detection of an unnatural linearly interrupted fog region inside the red circle. The daytime detection algorithm with visible/near infrared bands is used to the east of this line, and the ground surface is misidentified as fog. As mentioned above, reflectance corrected using SZA ($R_{B03}/\cos(SZA)$) is used for daytime fog detection. In Figure 9 (b), $R_{B03}/\cos(SZA)$ imagery shows brightness in the red circle because SZA is large, and the corrected reflectance is higher at sunrise/sunset. Thus, occurrence of false fog detection tends to increase at sunrise and sunset due to the excess of the low cloud extraction threshold ($R_{B03}/\cos(SZA) \geq 0.3$). In addition, if the NWP model predicts fine nighttime weather on land, the decrease in $n_{wp}T_{surf}$ due to radiative cooling and the consequent increase in $n_{wp}RH_{surf}$ may cause an excess in the threshold

for fog determination based on NWP data (e.g., $n_{wp}RH_{surf} \geq 85\%$). It is therefore presumed that the possibility of false detection on land is higher at sunrise than at sunset.

6. Development plans

Potential product improvements are outlined here.

6.1. Introduction of AI

As detailed above, the product identifies fog based on set thresholds with values derived from satellite observation and NWP. However, the current thresholds are based on subjective human judgment, and may not be optimal. Against this background, machine learning-based optimization for threshold setting may increase objectivity. The use of additional elements such as time-change information, peripheral grid information and topographical information may also be effective in this regard. Potential machine learning techniques include the Convolutional Neural Network (CNN) approach (e.g., Alzubaidi et al. 2021), which involves consideration of the spatial continuity of peripheral lattice observation values, and the LSTM (Long Short-Term Memory) approach (e.g., Van et al. 2020), which involves consideration of time-series observation values. Alternatives to building an original AI model include exploring suitable products such as CLAUDIA3 (Ishida et al. 2018), with which cloud areas

are determined using a support vector machine.

6.2. Introduction of Optimal Cloud Analysis (OCA)

Calvert and Pavolonis (2010) are among a number of researchers to have described calculation for derivation of cloud thickness based on cloud optical and microphysical properties determined from satellite observation. In this context, JMA is currently developing a product called Optimal Cloud Analysis (OCA) (Hayashi 2018), which may help to improve accuracy with incorporation of cloud properties. The product includes cloud top height information; if cloud thickness can be calculated, it is also possible to estimate cloud base height. This may facilitate more direct identification of fog areas (i.e., cloud bottom with ground contact).

6.3. Use of near-live ground fog observation data

Ground fog observation data and live camera images can also be used as near-live data for clear accuracy improvement.

7. Conclusion

This report describes JMA's Fog product, along with related usage, algorithms and accuracy. The product provides the following advantages:

- a) Fog areas can be determined over wide areas in 2D (including sea surface).
- b) Fog can be monitored virtually free of concerns over differences between day and night.
- c) High-probability fog areas can be displayed based on combination with NWP data.

As described in Chapter 6, the product still has significant potential for further development, which is currently being implemented for optimal output.

References

Alzubaidi, L., and Coauthors, 2021: Review of deep learning: Concepts, CNN architectures, challenges, applications, future directions. *Journal of big Data*, 8(1),

1-74.

Bessho, K., and Coauthors, 2016: An introduction to Himawari-8/9 — Japan's New-Generation Geostationary Meteorological Satellites. *J. Meteor. Soc. Japan*, **94**, 151-183.

Calvert, C., and M. Pavolonis, 2010: GOES-R Advanced Baseline Imager (ABI) algorithm theoretical basis document for low cloud and fog. NOAA NESDIS STAR, 78 pp, [available online at https://www.star.nesdis.noaa.gov/goesr/documents/ATBDs/Baseline/ATBD_GOES-R_Fog_v1.0_Sep2010.pdf] (Accessed 1 Sep 2022)

Ellrod, G. P., 1995: Advances in the detection and analysis of fog at night using GOES multispectral infrared imagery. *Wea. Forecasting*, 10, 606-619.

Hayashi, M., 2018: Introduction to the Computation Method for Cloud Radiative Processes and Its Application for the Advanced Himawari Imager onboard Himawari-8. Meteorological Satellite Center Technical Note, 63. (in Japanese with English abstract)

Ishida, H., and Coauthors, 2014: Investigation of Low-Cloud Characteristics Using Mesoscale Numerical Model Data for Improvement of Fog-Detection Performance by Satellite Remote Sensing. *Journal of Applied Meteorology and Climatology*, 53, 2246-2263.

Ishida, H., Oishi, Y., Morita, K., Moriwaki, K., Nakajima, T.Y., 2018. Development of a support vector machine based cloud detection method for MODIS with the adjustability to various conditions. *Remote Sens. Environ.* 205, 390–407.

JMA, 2022: Outline of the Operational Numerical Weather Prediction at the Japan Meteorological Agency. JMA, 261 pp. [Available online at <https://www.jma.go.jp/jma/jma-eng/jma-center/nwp/outline2022-nwp/index.htm>] (Accessed 1 Sep 2022)

Shimizu, A., Saitou, K., Yamamoto, M., 2017: Image characteristics of the 16 bands of Himawari-8's AHI. Meteorological Satellite Center Technical Note, 62, 39-71. (in Japanese with English abstract)

Shimizu, A., 2020: Introduction to Himawari-8 RGB composite imagery. Meteorological Satellite Center Technical Note, 65.

Van Houdt, G., and Coauthors, 2020: A review on the long short-term memory model. *Artificial Intelligence Review*, 53(8), 5929-5955.

Appendix: Glossary of terms

Term	Meaning
BXX	Himawari-8/9 band XX
R_{BXX}	BXX reflectance
T_{BXX}	BXX brightness temperature
SZA	Solar zenith angle
${}_{nwp}T_{sif}$	Predicted temperature on the ground
${}_{nwp}T_{700hPa}$	Predicted temperature at 700 hPa
${}_{nwp}RH_{sif}$	Predicted relative humidity on the ground
${}_{nwp}RH_{700hPa}$	Predicted relative humidity at 700 hPa
${}_{nwp}RH_{max(700/850/925hPa)}$	Maximum predicted relative humidity at 700/850/925 hPa

ひまわり 8 号霧監視プロダクトの開発

丸山拓海*¹ 石田春磨*² 中鉢幸悦*³

要旨

霧域の把握は航空機、船舶、自動車等の安全な交通のために重要である。霧域の監視において、海上も含めた広範囲に及ぶ面的な情報を得る手段としては、衛星観測が有効である。ただし、衛星は雲域を上空から観測するため、衛星観測のみから霧と下層雲(雲底が地表に接しているかいないか)を区別することは困難である。このため、気象庁では、ひまわり 8 号の観測データに加えて、地上付近の数値予報データの情報も考慮して霧の有無を判定し、面的な霧域の情報を提供する「ひまわり 8 号霧監視プロダクト」を開発した。本報告では、本プロダクトのアルゴリズム、精度、利用上の留意点等について記述する。

*¹ 気象庁大気海洋部業務課気象技術開発室

*² 気象研究所気象観測研究部

*³ 株式会社ハレックス

(2022 年 9 月 30 日受領、2022 年 10 月 25 日受理)